

1

2

3

4

**Dual role of striatal astrocytes in behavioral flexibility and metabolism in the context of obesity**

5

6

7

8

9

10 Enrica Montalban<sup>1\*</sup>, Daniela Herrera Moro Chao<sup>1</sup>, Anthony Ansoult<sup>1</sup>, Cuong Pham<sup>3</sup>,  
11 Andrea Contini<sup>2</sup>, Julien Castel<sup>1</sup>, Rim Hassouna<sup>1</sup>, Marene Hardonk<sup>1</sup>, Anna Petitbon<sup>2</sup>,  
12 Ewout Foppen<sup>1</sup>, Giuseppe Gangarossa<sup>1</sup>, Pierre Trifilieff<sup>2</sup>, Dongdong Li<sup>3,4</sup>, Serge  
13 Luquet<sup>1,4,5\*</sup>, Claire Martin<sup>1,4\*</sup>

14

15

16

17

18

\* corresponding authors:

19

[claire.martin@u-paris.fr](mailto:claire.martin@u-paris.fr) (C.M)

20

[serge.luquet@u-paris.fr](mailto:serge.luquet@u-paris.fr) (S.H.L.)

21

[enrica.montalban@gmail.com](mailto:enrica.montalban@gmail.com) (E.M.)

22

23

24

<sup>1</sup>Université Paris Cité, CNRS, Unité de Biologie Fonctionnelle et Adaptative, F-75013 Paris, France.

25

26

<sup>2</sup>Univ. Bordeaux, INRAE, Bordeaux INP, NutriNeuro, UMR 1286, F-33000, Bordeaux, France

27

<sup>3</sup>Institute of Biology Paris Seine, Neuroscience Paris Seine, CNRS UMR8246, INSERM

28

U1130, Sorbonne Université, 75005, Paris, France

29

<sup>4</sup>Senior authors

30

<sup>5</sup>Lead contact

31

32

33

34

35 **ABSTRACT**

36

37 Brain circuits involved in metabolic control and reward-associated behaviors are potent  
38 drivers of feeding behavior and are both dramatically altered in obesity, a multifactorial  
39 disease resulting from genetic and environmental factors. In both mice and human, exposure  
40 to calorie-dense food has been associated with increased astrocyte reactivity and pro-  
41 inflammatory response in the brain. Although our understanding of how astrocytes regulate  
42 brain circuits has recently flourish, whether and how striatal astrocytes contribute in  
43 regulating food-related behaviors and whole-body metabolism is still unknown. In this study,  
44 we show that exposure to enriched food leads to profound changes in neuronal activity and  
45 synchrony. Chemogenetic manipulation of astrocytes activity in the dorsal striatum was  
46 sufficient to restore the cognitive defect in flexible behaviors induced by obesity, while  
47 manipulation of astrocyte in the nucleus accumbens led to acute change in whole-body  
48 substrate utilization and energy expenditure. Altogether, this work reveals a yet  
49 unappreciated role for striatal astrocyte as a direct operator of reward-driven behavior and  
50 metabolic control.

51

52

53 **KEYWORDS**

54 Astrocytes, behavior, obesity, cognitive flexibility, dorsal striatum, nucleus accumbens,  
55 synchrony, metabolism, fatty acid oxidation

56

## 57 Introduction

58 Obesity is a major public health problem, which increases the relative risk of a set of  
59 pathological conditions (e.g. heart disease, hypertension, type 2 diabetes, steatosis and  
60 some form of cancers) (Must et al., 1999; GBD 2015 Obesity Collaborators et al., 2017).  
61 Although both genetic and lifestyle factors thoroughly participate in the development of  
62 obesity, the contribution of each factor widely varies from individual to individual. Over  
63 consumption of highly rewarding high fat, high sugar diet (HFHS) is definitively an identified  
64 culprit. While homeostatic circuits located in the hypothalamic-brainstem axis are potent  
65 contributors of feeding behaviors, the rewarding nature of food is another powerful drive of  
66 feeding (Berthoud et al., 2017). The rewarding aspect of food involves the release of  
67 dopamine (DA) within the cortico-mesolimbic system (Berridge, 1996; Alcaro et al., 2007;  
68 Björklund and Dunnett, 2007). Consumption of HFHS enhances DA release within the  
69 Nucleus accumbens (NAc) and the dorsal striatum (DS) (Lenoir et al., 2007), which in turn  
70 influences the striato-hypothalamic circuits promoting food intake (Kenny, 2011; Kempadoo  
71 et al., 2013; O'Connor et al., 2015). Alterations in the DA transmission have been shown to  
72 be implicated in addictive/compulsive-like ingestive behaviors as well as altered cognitive  
73 flexibility (Yang et al., 2018) and reward processing (Koob and Volkow, 2010), two well-  
74 established endophenotypes of overweight individuals, which largely depend on striatal  
75 processing. It is therefore suggested that, by hijacking the reward system, exposure to  
76 palatable hypercaloric diets can switch feeding from a goal-directed and flexible behavior, to  
77 an impulsive (Babbs et al., 2013; Adams et al., 2015), inflexible, and ultimately compulsive-  
78 like behavior [see (Wang et al., 2001; Johnson and Kenny, 2010; Kenny, 2011; Michaelides  
79 et al., 2012)]. In line with this, increasing evidence support that the development of obesity  
80 and obesity-related disorders not only results from metabolic dysregulation, but also from  
81 dysfunctions of the fronto-striatal circuit, a main substrate for inhibitory behaviors and  
82 cognitive control, which can be altered in response to food and associated cues (Stice et al.,  
83 2008; Seabrook et al., 2023). However, the cellular and molecular events that underlie the  
84 mal adaptive response of the reward system to obesogenic environment remain elusive.

85 Increasing evidence point to an alteration of astrocytes, the most abundant type of glial cells  
86 (García-Cáceres et al., 2019), as a pathophysiological feature of obesity. Astrocytes  
87 reactivity, reflected by both morphological and functional remodeling has already been  
88 described in the hypothalamus, in response to days or weeks of HFHS exposure, well before  
89 fat accumulation and systemic inflammation (Thaler et al., 2012; Clyburn and Browning,  
90 2019). Consumption of enriched diet and the excess of adipose tissue further favor  
91 inflammatory cascades associated with secretion of pro-inflammatory signals (Thaler et al.,

92 2012), triggering vascular hyper permeability and maladaptation in both microglia and  
93 astrocytes (García-Cáceres et al., 2019).

94 Despite the physiological evidence that astrocyte are primary target of caloric dense food, it  
95 is yet unclear if they play a dominant role in the cognitive and metabolic defect associated  
96 with obesity. In the current study, we show that long-term exposure to HFHS leads to  
97 profound changes in striatal astrocytes states and activity, associated with loss of synchrony  
98 in neuronal activity and impairs mice reversal learning. Second, we show that selective  
99 manipulation of striatal astrocyte through chemogenetic approaches helps reinstate neural  
100 network coordination. Third, we identified a neuroanatomical distinction by which activation of  
101 astrocytes in the dorsal striatum can directly rescue HFHS diet-induced cognitive dysfunction  
102 while manipulating astrocytes activity in the Nucleus accumbens exert a dominant control  
103 onto whole-body substrate utilization and energy expenditure.

## 104 **Results**

### 105 **High-fat diet-induced obesity leads to reactive astrocytes in both the Nucleus** 106 **Accumbens and the Dorsal Striatum.**

107 Previous studies have demonstrated that HFHS exposure results in reactive astrocytes  
108 (Douglass et al., 2017) and alters astrocytic calcium signals in the hypothalamus (Herrera  
109 Moro Chao et al., 2022). Anatomical and functional studies have suggested a functional  
110 heterogeneity within the striatum, with the ventral striatal regions more likely to be involved in  
111 goal directed behaviors, and the dorsal subdivisions rather related to motor control and  
112 habits development (Kravitz and Kreitzer, 2012; Lee et al., 2012). Therefore, we explored the  
113 distinctive astrocytic adaptations in both the DS and the NAc. Mice were exposed to HFHS  
114 for a minimum of 3 months (**Fig-1A**), leading to a significant increase in fat mass compared  
115 to chow fed littermates (**Fig-1A**). In both NAc and DS, exposure to HFHS diet enhanced  
116 immunoreactivity of the structural protein glial fibrillary acidic protein (GFAP) (**Fig-1B,C,F**), a  
117 proxy of increased astrocyte reactivity (Escartin et al., 2021). In HFHS fed mice, the increase  
118 in GFAP signal intensity was also accompanied by a decrease in the sphericity of the  
119 segmented GFAP positive regions in both the DS and the NAc (**Fig-1D,G**), indicating an  
120 effect of HFHS diet on astrocytes morphology. In HFHS-fed groups, the total surface of  
121 GFAP staining was significantly increased in the NAc indicating an increase of astrocytic  
122 coverage, (**Fig-1E**) while unchanged in the DS (**Fig-1H**). Altogether, these data indicate a  
123 functional heterogeneity in the striatal astrocyte response to HFHS diet exposure.

124 **Chemogenetic manipulation of DS astrocytes affects spiny projections neurons**  
125 **activity**

126 The finding that HFHS exposure triggers structural and functional changes in striatal  
127 astrocytes led us to assess metabolic and behavioral consequences of astrocytic  
128 manipulation in the striatum of lean and obese mice. We first probed the consequence of  
129 chemogenetic (Designed Receptors Exclusively activated by Designer Drug)-mediated  
130 manipulation of DS astrocytes on DA signaling mediated by pharmacological intervention  
131 onto dopamine 1 receptor (D1R) and dopamine 2 receptor (D2R). Lean and obese mice  
132 expressing the CRE recombinase under the control of the astrocytes-specific promoter  
133 Aldehyde dehydrogenase family 1, member L1 (Aldh1l1-Cre) (Cahoy et al., 2008) were  
134 stereotactically injected with Cre-dependent pAAV-EF1 $\alpha$ -DIO-hM3Dq-mCherry in the DS  
135 allowing for the astrocyte-specific expression of the Gq-coupled receptor (DS<sup>hM3Dq</sup>) (**Supp.**  
136 **Fig-1**). Astrocytic-specific targeting was confirmed by co-immunolocalization of the mCherry  
137 signal in striatal astrocytes with the astrocyte's marker GFAP (**Supp. Fig-1A**). Next, to  
138 validate the DREADD-induced Ca<sup>2+</sup> signaling in astrocytes, we co-expressed the Ca<sup>2+</sup>  
139 indicator GCaMP6f using Cre-dependent AAV vector. Intraperitoneal injection (IP) of the  
140 DREADD ligand Clozapine N-Oxide (CNO, 0.6 mg/kg) led to significant increase of astrocytic  
141 Ca<sup>2+</sup> activity as assessed *in vivo* through fiber photometry recording of DS GCaMP6-based  
142 fluorescence (**Supp. Fig-1B, C**). As a functional readout, we observed that Gq-DREADD-  
143 mediated manipulation of astrocytes in the in DS astrocyte did not alter hyper locomotion  
144 triggered by a single injection of the D1R agonist (SKF-81297) (**Supp Fig-1D**), while the  
145 cataleptic effects induced by the D2R antagonist haloperidol (0.5 mg/kg) was significantly  
146 decreased in response to the DREADD ligand CNO. Interestingly, this effect was further  
147 enhanced in obese mice (**Supp. Fig-1E-F**).

148 **Diet-induced obesity leads to increased temporal correlation of astrocyte Ca<sup>2+</sup> signals**  
149 **in the DS**

150 Next, we investigated how HFHS exposure impacts onto spontaneous astrocytic Ca<sup>2+</sup>  
151 dynamics, an important feature of astrocyte signalling (Aguilhon et al., 2008; Khakh and  
152 McCarthy, 2015). To do so, we used mice expressing the genetically encoded Ca<sup>2+</sup> sensor  
153 GCaMP6f under the astrocyte-specific promoter of the glutamate-aspartate transporter  
154 (*Slc1a3*, GLAST) (Glast-GCaMP6f), (Pham et al., 2020; Herrera Moro Chao et al., 2022).  
155 Wide-field imaging of striatal astrocytes in acute brain slices of lean and obese Glast-  
156 GCaMP6f mice showed that exposure to HFHS does not affect Ca<sup>2+</sup> spontaneous activity in  
157 the DS (**Fig-2A**). However, in the DS, obesity associates with an increased temporal  
158 correlation of astrocyte Ca<sup>2+</sup> signals, as showed by calculating the paired Pearson's

159 coefficient, a correlation coefficient between individual  $\text{Ca}^{2+}$  signals reflecting signal  
160 synchronicity. While the distribution of temporal correlation of  $\text{Ca}^{2+}$  signals from all active  
161 domains appeared bimodal in lean mice, suggesting that astrocyte  $\text{Ca}^{2+}$  signals are  
162 segregated into two populations of asynchronous temporal features, this distribution is right  
163 shifted in obese mice indicating increased temporal correlation (**Fig-2B**). These results show  
164 that beyond a change of astrocyte  $\text{Ca}^{2+}$  signaling intensity, exposure to HFHS changes the  
165 temporal organization of astrocyte activation. Because astrocytes are tightly linked with  
166 synaptic activity, it is likely that this shift also affects neuronal synchronization.

### 167 **DS astrocytes chemogenetic manipulation in obese mice rescues neuronal** 168 **synchronization**

169 Using brain slice preparation for GCaMP6f monitoring we observed that obesity had little  
170 impact on the overall strength of neuronal  $\text{Ca}^{2+}$  signals (**Supp. Fig-2A**), but significantly  
171 decreased temporal correlation pattern of neuronal events and reduced on average their  
172 correlation level as compared to lean animals (**Fig-3B**), suggesting that obesity compromised  
173 the synchrony in the DS neuronal network. To further explore the impact of obesity on  
174 astrocyte-neuron communication in the DS, we examined the effect of astrocytes  
175 chemogenetic manipulation on neuronal  $\text{Ca}^{2+}$  signals *ex vivo*. C57Bl6 mice received a  
176 mixture of viral vectors allowing for simultaneous expression of GCaMP6f in neurons (AAV-  
177 synapsin-GCaMP6f) and hM3Gq in astrocytes (AAV-GFAP-hM3Gq-mCherry) (**Fig-3A**).  
178 Next, we analyzed neuronal time courses during Gq-DREADD astrocyte activation in lean  
179 and obese animals. We first validated that coincident activation of neuronal populations can  
180 enhance their synchrony. To do so, we used glutamate whose receptors are abundantly  
181 expressed in DS neurons (Montalban et al., 2022) and applied a concentration (30 $\mu\text{M}$ ) that  
182 targets perisynaptic mGluR and/or NMDA receptors, hence mimicking the activation of  
183 glutamate receptors targeted by Gq-DREADD astrocyte activation. Application of glutamate  
184 did synchronize the  $\text{Ca}^{2+}$  events in GCaMP6f-expressing DS neurons, as reflected by  
185 simultaneous fluorescence rises (**Supp. Fig-2B, C**) and the right shifted distribution of the  
186 temporal correlations (**Supp. Fig-2D, E**).

187

### 188 **Activation of DS astrocytes rescues neuronal synchronization defect associated with** 189 **obesity**

190

191 We then examined whether Gq-mediated activation of DS astrocytes could modulate  
192 neuronal activity profile as assessed by GCaMP6f activity. Bath application of CNO

193 significantly increased the level of temporal correlation between neuronal  $\text{Ca}^{2+}$  signals,  
194 leading to a right shift of the correlation distribution (**Fig-3C-D**). Notably, the impairment of  
195 neuronal  $\text{Ca}^{2+}$  signals synchrony associated with obesity was largely restored by Gq-  
196 DREADD-mediated astrocytes activation (**Fig-3D**), along with overall enhancement of  
197 neuronal activity (**Fig-3E**). To further confirm this effect, Aldh111-Cre mice were co-injected  
198 with Gq-DREADDs or mCherry control viruses ( $\text{DS}^{\text{mCherry}}$  and  $\text{DS}^{\text{hM3Dq}}$ ) and AAV-synapsin-  
199 GCaMP6f to target neurons. As previously observed, the strength (**Supp. Fig-3A-B**) and  
200 temporal correlation (**Supp. Fig-3C**) of DS neuronal  $\text{Ca}^{2+}$  signals were increased by both  
201 glutamate bath application and CNO-mediated DREADD manipulation of astrocytes.  
202 Together, these results show that the signal synchronization of DS neurons is dampened in  
203 obese mice, but can be restored by selective activation of striatal astrocytes.

204

205 **Obesity-associated impairment in cognitive flexibility can be rescued by selective**  
206 **activation of striatal astrocyte.**

207 We next explored the functional outcome of DS astrocytes manipulation onto obesity-induced  
208 cognitive alteration. Reversal learning is a form of cognitive flexibility highly dependent on to  
209 the integrity of the DS and that was shown to be impaired in human and rodent obesity (Foldi  
210 et al., 2021; Montalban et al., 2023). Neuroimaging studies in humans show that reversal  
211 learning requires the integrity of the ventral prefrontal cortex and the DS (Jocham et al.,  
212 2009). Previous studies already showed that activation of astrocytes in the DS facilitate the  
213 switch from habitual to goal directed behavior in lean mice in a operant conditioning  
214 paradigm (Kang et al., 2020). We first evaluated if DS-dependent flexible behavior was  
215 altered in obese mice. To do so, lean and obese mice of matched age were tested in a food-  
216 cued T-maze, in which mice learnt to locate the baited arm with no external cues, using an  
217 egocentric strategy (Oliveira et al., 1997; Watson and Stanton, 2009; Baudonnat et al., 2013)  
218 followed by a reversal learning task, in which locations of the baited and non-reinforced arms  
219 are inverted (**Fig-4A**). While no differences were observed during the learning phase, obese  
220 mice displayed impaired ability to relearn the new location of the baited arm during reversal  
221 task (**Fig-4A**). Their performances did not reach criterion even after 3 sessions of reversal  
222 test (**Supp. Fig-4**) whereas lean mice reached 80% of correct choice during the first reversal  
223 session (**Fig-4A**).

224 Next, we assessed the consequence of Gq-DREADDs activation of DS astrocyte on reversal  
225 learning in lean and obese Aldh111  $\text{DS}^{\text{mCherry}}$  and  $\text{DS}^{\text{hM3Dq}}$  mice. Reversal learning was  
226 assessed in response to CNO injection 30 minutes before the first trial of the reversal phase

227 **(Fig-4B, C)**. Importantly, while activation of Gq-DREADD in DS astrocytes in lean mice led to  
228 a small though significant increased performance **(Fig-4B)**, CNO injection in obese DS<sup>hM3Dq</sup>  
229 led to an almost complete restoration of reversal learning during the reversal phase **(Fig-4C)**.  
230 Our results indicate that DS astrocytes activation during reversal learning was sufficient to  
231 restore obesity-induced impairment in cognitive flexibility.

232 **Astrocyte-mediated restoration of flexible behavior in obese mice is associated with**  
233 **changes in both neuronal activity and dopamine transmission *in vivo***

234 In order to link the behavioral output with bulk neuronal activity in the DS upon Gq-DREADD  
235 astrocytes activation *in vivo*, we recorded neuronal activity using Ca<sup>2+</sup> sensor coupled with  
236 fiber photometry during reversal learning. Our analysis showed that astrocytes activation  
237 during reversal learning was accompanied by a small decrease of neuronal activity when the  
238 animal enters the baited arm in obese DS<sup>hM3Dq</sup> as compared to DS<sup>mCherry</sup> **(Fig-4D-G)**.

239 Several studies indicate that obesity and HFHS exposure enhances DA signaling in both  
240 humans (Volkow and Wise, 2005) and rodents (Johnson and Kenny, 2010; Tellez et al.,  
241 2013), and recent studies point to a role of astrocytes in regulating the level of DA release in  
242 the striatum (Roberts et al., 2022). Since DA transmission regulates behavioral flexibility  
243 (Izquierdo et al., 2017), we investigated the role of DS astrocytes in DA transmission during  
244 the reversal learning. Obese DS<sup>mCherry</sup> and DS<sup>hM3Dq</sup> mice were co-injected with a viral vector  
245 bearing the genetically-encoded DA sensor dLight1 in the DS (AAV-CAG-  
246 dLight1.1)(Patriarchi et al., 2018). Fiber photometry recording of dLight1-mediated signal was  
247 used as a proxy of DA dynamics in the DS. Mice were first recorded during a reversal  
248 learning after being injected with vehicle (RV1, **Fig-4H-J**) and, next, during a second reversal  
249 learning after being injected with CNO (RV2, **Fig-4H-J**). Our analysis showed that astrocytes  
250 activation during reversal learning potentiated DA transmission when the animal entered the  
251 baited arm **(Fig-4I, J)**.

252 Overall our data showed that in DS astrocytes activation in obese mice restores reversal  
253 learning impairments in relation with i) an overall decrease in neuronal activity and ii) an  
254 increase in DA transmission when entering the new-bated arm during reversal learning.

255

256 **Diet induced obesity leads to increased strength and decreased temporal correlation**  
257 **of astrocyte Ca<sup>2+</sup> signals.**



258 Converging evidence point to a central role of the ventral part of the striatum in the regulation  
259 of food intake (Sears et al., 2010; O'Connor et al., 2015; Thoeni et al., 2020), glucose  
260 metabolism (Ter Horst et al., 2018) and whole body substrate utilization (Montalban et al.,  
261 2023). Hence, we next considered a possible role of NAc astrocytes in the physiology and  
262 pathophysiology of energy balance in obesity.

263 First, we investigated the effect of HFHS exposure on spontaneous activity of NAc astrocytes  
264 in GLAST-GCaMP6f mice. Interestingly, we found that contrarily to the DS, exposure to  
265 HFHS led to a significant increase in NAc astrocytic  $Ca^{2+}$  spontaneous activity (**Fig-5A**).  
266 Moreover, as for the DS, lean mice showed a bimodal  $Ca^{2+}$  distribution suggesting that  
267 astrocyte  $Ca^{2+}$  signals are segregated into two populations of asynchronous temporal  
268 features (**Fig-5B**). However, in contrast to the DS, exposure to HFHS diet led to a left  
269 monomodal distribution in the NAc, indicating a decrease in astrocytes synchronization (**Fig-**  
270 **5B**). We next examined the effect of astrocyte activation in Aldh111-cre mice that received  
271 intra NAc delivery of Cre-dependent viral vectors encoding for Gq DREADD and GCaMP6f.  
272 We observed a significant increase in NAc astrocyte  $Ca^{2+}$  levels following CNO bath  
273 application in lean mice (CNO, 10 $\mu$ M) (**Supp. Fig-5A, B**). This observation led us to  
274 hypothesize that Gq-DREADD-mediated increase of astrocytic  $Ca^{2+}$  in the NAc of obese mice  
275 would have little effect as compared to stimulation of astrocytes in lean mice. We used  
276 pharmacology to assess whether astrocytes manipulation would influence behavioral  
277 response to agonist and antagonist of D1R and D2R. We observed that NAc astrocytes  
278 activation opposed SKF-81297 (3mg/kg) induced hyperlocomotion in lean mice, while this  
279 effect was dampened in obese mice (**Supp. Fig-5D, E**). In contrast to DS, astrocytes  
280 activation in the NAc did not trigger any significant effects in the cataleptic response to the  
281 D2R antagonist haloperidol (0.5 mg/Kg) (**Supp. Fig-5C**) further supporting segregated  
282 function of NAc vs DS astrocyte.

### 283 **Astrocytes activation in the Nucleus accumbens impacts on peripheral substrate** 284 **utilization**

285 We then assessed changes in metabolic efficiency in lean and obese Aldh111-Cre mice co-  
286 injected with Gq-DREADDs or mCherry viruses (NAc<sup>mCherry</sup> and NAc<sup>hM3Dq</sup>) and AAV-synapsin-  
287 GCaMP6f by monitoring indirect calorimetry in response to CNO-mediated astrocytes  
288 manipulation (**Fig-6A**). In lean mice, acute stimulation of NAc astrocytes only marginally  
289 affected feeding (**Fig-6B**), but promoted a significant decrease in respiratory exchange ratio  
290 (RER,  $VCO_2/VO_2$ ) indicative of substrate being used with RER=1 for carbohydrate and  
291 RER=0.7 for lipids (**Fig-6C**). Correlation studies indicated that such decrease in RER  
292 significantly correlated with food consumption in Aldh111 NAc<sup>Gq</sup> group (**Fig-6D**). In

293 accordance, the calculated whole body fat oxidation (Fat Ox) confirmed that acute activation  
294 of astrocytes in the NAc led to a shift towards lipid-based substrate (**Fig-6E**). While whole  
295 body metabolism (**Supp. Fig-6**) remained unaffected by activation of DS astrocyte in both  
296 lean and obese DS<sup>mCherry</sup> or DS<sup>hM3Dq</sup> mice, chemogenetic manipulation of NAc astrocytes also  
297 resulted in a decrease of energy expenditure (EE) (**Fig. 6F**). This effect was independent  
298 from the mice lean body mass (**Fig-6G**) and locomotor activity, which are not different  
299 between groups (**Fig-6H**). In obese mice however, activation of astrocytes in the NAc did not  
300 alter either food intake, RER, FatOx or EE (**Fig-6I-L**), further supporting the notion that  
301 obesity led to maladaptive response in astrocytic control of metabolism.

302

### 303 **Discussion**

304

305 In the context of the obesity pandemic, the striatum has attracted increasing attention, as  
306 energy-rich diets are known to promote reward dysfunctions by altering DA transmission  
307 within both NAc and DS. Such alterations can lead to maladaptive habits formation, food  
308 craving, inability to cut down food intake and, ultimately to body weight gain. However, while  
309 the role of striatal neurons is actively investigated, the contribution of striatal astrocytes in the  
310 development of metabolic defects is still largely overlooked. Here, we tested the hypothesis  
311 that i) in a diet-induced obesity paradigm striatal astrocytes could be a major target of  
312 nutrient overload and that ii) manipulation of astrocytes in DS or NAc could restore  
313 behavioral and metabolic alterations induced by obesity. Consistently, we show that obesity  
314 induces anatomically-specific change in astrocyte reactivity characterized by substantial  
315 alteration in their morphology in both NAc and DS, recalling the modifications observed in the  
316 hypothalamus (Thaler et al., 2012). Further, we showed that HFHS consumption translates in  
317 an anatomically restricted change in overall Ca<sup>2+</sup> strength in NAc astrocytes but not in DS  
318 astrocytes. In contrast, while temporal correlation in astrocytes Ca<sup>2+</sup> events was similar in  
319 NAc and DS in lean mice, HFHS exposure led to a shift towards a monomodal Ca<sup>2+</sup> events  
320 distribution in the NAc (decreased synchronization), and a significant increase in temporal  
321 correlation as compared to lean mice in the DS. Those findings highlight that the functional  
322 heterogeneity of astrocytes may reflect different kind of activations among or within brain  
323 regions according to their interactions with different subpopulations of neurons (Khakh and  
324 Sofroniew, 2015).

325

326 Obesity is a condition characterized by both metabolic and behavioral alterations. Among the  
327 latter, non-flexible behavior is a symptomatic dimension which is well characterized in obese

328 subjects. Here we measured reversal learning, a dimension known to be particularly affected  
329 in obese subjects, relying on an egocentric-based strategy, a process highly dependent on  
330 the integrity of DS (van Elzelingen et al., 2022), and that requires the integrity of the ventral  
331 prefrontal cortex and DS (Jocham et al., 2009). Using chemogenetics, we showed that  
332 activation of DS-astrocytes in lean and obese mice facilitate flexible behavior during the  
333 reversal learning phase of a T-maze task. In obese mice, astrocyte activation was sufficient  
334 to restore learning flexibility during reversal. These data are in line with a key role of the DS  
335 astrocytes in the switch from habitual to goal directed behavior (Kang et al., 2020), and  
336 highlight a central role of astrocytes for the long-term consequences of obesity. Using both  
337 chemogenetics, GCaMP6f and d-Light based imaging of neural activity and DA transmission  
338 *in vivo*, we showed that in obese mice the reinstatement of a flexible behavior under  
339 astrocytes activation parallels with a general decrease in neuronal activity in the DS together  
340 with an increase in DA transmission during the choice phase, i.e. when mice are entering the  
341 rewarded arm. Dysfunctional DA transmission is associated to several psychiatric  
342 pathologies characterized by alterations in flexible behavior (Insel et al., 2010; van Elzelingen  
343 et al., 2022). These data confirm that reestablishing the DA transmission within the DS  
344 correlates with a gain in the ability to adapt its behavior (Leroi et al., 2013) and are in line  
345 with previous reports showing that astrocytes are active players in DA signaling in the  
346 striatum (Martín et al., 2015; Corkrum et al., 2020)

347 In line with this, we found that i) obesity is accompanied with a sharp decrease of  $Ca^{2+}$   
348 dynamics synchronization in spiny projection neurons SPNs of the DS, that ii) astrocytes  
349 activation can restore neural  $Ca^{2+}$  event synchronicity, and that iii) in obese mice glutamate  
350 application can mimic chemogenetic activation of astrocytes by restoring neural  $Ca^{2+}$  events  
351 synchrony. These data extend previous works showing that astrocytes can modulate  
352 neuronal networks excitability and switch dynamic states *ex vivo* and *in vivo* (Fellin et al.,  
353 2004; Poskanzer and Yuste, 2011, 2016; Oliveira and Araque, 2022). Synchronized activity  
354 is a defining feature of the nervous system that correlates with brain functions and behavioral  
355 states. Several brain diseases are associated with abnormal neural synchronization (Uhlhaas  
356 and Singer, 2006). In the striatum, rearrangement in neuronal synchronization plays a key  
357 role in habitual learning (Howe et al., 2011; Thorn and Graybiel, 2014; Smith and Graybiel,  
358 2016), hence it is tempting to propose that modulation of synchrony by astrocytes translates  
359 into the modifications of behavior that we observed in our experiments. Gq-DREADDs  
360 activations and concurrent  $Ca^{2+}$  increase can have many consequences on is the so-called  
361 the tripartite synapse (Araque et al., 1999). Astrocytes release and uptake neuroactive  
362 molecules that could impact both pre- and postsynaptic neuronal functions (Leybaert and  
363 Sanderson, 2012; Orellana et al., 2016; Savtchouk and Volterra, 2018)- an effect that have  
364 been already suggested in the NAc (D'Ascenzo et al., 2007). Astrocytes are also known to

365 shape synaptic activity and communication by precisely buffering the level of extra synaptic  
366 glutamate concentration (Isaacson, 1999; Martin et al., 2012). In this study we observed that  
367 in obese but not lean mice, glutamate application increased neuronal synchrony. Since  
368 glutamate or CNO application, and CNO glutamate co-application resulted to comparable  
369 effects in acute slices from obese mice, a possibility would be that in the DS, obesity would  
370 result in a deregulation of glutamate reuptake from astrocytes, an effect that could be  
371 rescued by astrocytes activation. Hence, at mechanistic level, our data suggest a central role  
372 for astrocyte in controlling neural  $Ca^{2+}$  events synchrony and DA transmission. Altered  
373 regulation of glutamate in obesity is a mechanism reminiscent of our recent study that  
374 depicted a key role for hypothalamic astrocyte in the regulation of neurons firing ability,  
375 energy expenditure and glucose metabolism through the control of ambient glutamate  
376 (Herrera Moro Chao et al., 2022). We found that obesity was associated with exacerbated  
377 astrocyte  $Ca^{2+}$  activity and blunted astrocyte-selective excitatory Amino-Acid Transporters  
378 (EAATs)-mediated transport of glutamate (Herrera Moro Chao et al., 2022). Since a large  
379 portion (~ 80%) of glutamate released is actively recaptured by astrocyte through Glutamate  
380 transporter 1 (GLT-1) and EAATs transporters, it is expected that striatal astrocyte will have  
381 a key role in the control of glutamate in the striatum. Indeed, it was recently demonstrated  
382 that glutamate transporter in the astrocytes was in control of Hebbian plasticity expression in  
383 the SPNs in the DS (Valtcheva and Venance, 2016).

384

385 In line with emerging evidence that point at the connection between the DA circuits and  
386 metabolic control (Montalban et al., 2023) , we found that, activation of NAc astrocytes in  
387 lean mice led to significant shift towards lipids substrate utilization. Given the connection  
388 between the NAc and hypothalamic nuclei involved in metabolic control, notably the lateral  
389 part of the hypothalamus (LHA) (Stratford and Kelley, 1999; Sears et al., 2010; O'Connor et  
390 al., 2015; Thoeni et al., 2020) it is formally possible that NAc astrocytes activity indirectly  
391 impede onto a subset of neurons projecting to the LHA, with consequences on hypothalamic  
392 control of energy expenditure and lipids metabolism (Farzi et al., 2018). This hypothesis is  
393 consistent with previously proposed role for a hypothalamic-thalamic-striatal axis in the  
394 integration of energy balance and food reward (Kelley et al., 2005). In obese mice, activation  
395 of astrocytes of the NAc failed to affect energy metabolism suggesting impaired astrocyte-  
396 neural coupling induced by obesity, possibly through astrocyte over activity. Indeed, our *ex*  
397 *vivo* studies showed that Gq-coupled hM3Dq activation in astrocyte leads to increases  $Ca^{2+}$   
398 signals similar to the one observed in obese conditions. Therefore, it is tempting to  
399 hypothesize that activation of astrocytes in the NAc of lean mice would mimic at least in part  
400 some of the obesity metabolic dimensions similarly to what has been observed in  
401 hypothalamic astrocyte (Herrera Moro Chao et al., 2022).

402 Our data support the notion that the physiological outcome arising from astrocyte  
403 manipulation will strongly depend on the anatomical localization and the way astrocyte  
404 interacts with different subpopulations of neurons (Khakh and Sofroniew, 2015). Indeed,  
405 while CNO-mediated activation of Gq-coupled DREADD astrocytes in the DS had marginal  
406 effect on metabolic efficiency, chemogenetic activation of the NAc astrocyte in lean mice  
407 decreased energy expenditure and sustained change in nutrient partitioning interpedently from  
408 caloric intake. In the same concept, chemogenetic manipulation of DS astrocytes decreased  
409 the cataleptic effects induced by the D2R antagonist haloperidol but did not affect  
410 hyperlocomotion response to D1R agonist SKF-81297 suggesting a bias action of astrocyte  
411 towards D2R-bearing cells. This result was mirrored in the NAc in which hyperlocomotion  
412 response to D1R agonist but not cataleptic response to D2R antagonist was affected by the  
413 activation of hM3Dq in the NAc astrocyte. These data directly point at a segregated action of  
414 astrocyte in the dichotomic action onto specific neuronal population and DA receptor  
415 signaling likely due to the selective and anatomically defined properties of astrocyte-neurons  
416 communication. For instance in the DS, two distinct subpopulation of astrocytes have been  
417 identified that communicate selectively with D1R or D2R-SPNs (Martín et al., 2015). In  
418 addition to this intrinsic diversity in astrocyte-neurons communication, our study highlights  
419 that exposure to caloric dense food differently affects astrocyte-neuron communication in  
420 NAc and DS. While the consequence of NAc astrocyte activation onto metabolic efficiency  
421 observed in lean mice was mitigated by obesity, the cognitive improvement associated with  
422 DS astrocyte activation was magnified in obese mice. Here too, the differential impact of high  
423 fat feeding might reflect the intrinsic diversity in adaptive response to metabolic signals in DS  
424 vs NAc astrocyte, neurons, or both astrocyte-neurons tandem.

425 In conclusion, this study provides a ground for a more astrocentric vision of diet and obesity  
426 induced alteration in cognitive and metabolic function and open new therapeutic avenue in  
427 which striatal astrocytes could represent potential target to correct behavioral and metabolic  
428 diseases. However, in order to fully harvest the therapeutic potential of an astrocytic-specific  
429 target strategy there is a critical need to further expand our knowledge in molecular  
430 specificity and mechanism that sustain astrocyte-neuron dialogue in both physiological and  
431 pathophysiological condition based on their anatomical distribution.

432

### 433 **Limitations of the study**

434 Due to paucity of tools readily available to characterize DS or NA astrocyte diversity, our  
435 study could not provide a more detailed description of the specific features of astrocytes  
436 involved in the described mechanism. Further, while changes in astrocytic or neural  $Ca^{2+}$   
437 events are indicative of cell response they most likely coexist with other intracellular changes  
438 that are not accounted for in our study. Further studies are needed to establish the molecular

439 transmitters, metabolite or metabolic pathways that are engaged in astrocyte-neurons  
440 connection and which of them represent the best target to leverage as future strategy to cope  
441 for diet-induce metabolic and cognitive disease.

442

443 --end--

444

445

#### 446 **AUTHORS CONTRIBUTION**

447 E.M. initiated, developed and supervised the project, designed and performed experiments,  
448 analyzed and interpreted the data, prepared figures and wrote the original draft. CM  
449 supervised and developed the research, designed and performed in vivo experiments,  
450 analyzed and interpreted the data, prepared figures and participated in the writing of the  
451 manuscript with the help of the co-authors. SHL provided the initial conception of the project,  
452 secured and administered funding, provided guidance for experimental design and data  
453 interpretation and contributed to the writing of the manuscript with the help of the co-authors.  
454 DL designed and performed ex-vivo calcium imaging experiments, analyzed and interpreted  
455 the data, prepared figures and participated in the writing of the manuscript. PT contributed to  
456 analysis and interpretation of the data and writing of the manuscript. GG contributed to the  
457 design and provided inputs to in vivo experiments and discussed the data. DHMC and CP  
458 performed ex-vivo calcium imaging experiments, AC, AP, PT contributed to fiber photometry  
459 experiments. DHMC, AA, JC, RH, MH, EF contributed to in vivo experiments and  
460 immunohistochemistry.

461

#### 462 **ACKNOWLEDGEMENTS**

463 We acknowledge funding supports from l'Agence Nationale de la Recherche (ANR) ANR-19-  
464 CE37-0020-02, ANR-20-CE14-0020, and ANR-20-CE14-0025-01 "AstrObesity" and from the  
465 Fondation pour la Recherche Médicale (FRM) FRM Project #EQU202003010155. We thank  
466 the Université Paris Cité, CNRS, INRAE and Université de Bordeaux. EM was supported by  
467 a post-doctoral fellowship from the FRM and awarded by the « Fondation des Treilles ». « La  
468 Fondation des Treilles, créée par Anne Gruner-Schlumberger, a pour vocation de nourrir le  
469 dialogue entre les sciences et les arts, afin de faire progresser la création et la recherche.  
470 Elle accueille des chercheurs et des créateurs dans son domaine des Treilles (Var) [www.les-treilles.com](http://www.les-treilles.com) ». We thank Olja Kacanski for administrative support, Isabelle Le Parco, Aurélie  
471 Djemat, Daniel Quintas, Magguy Boa Ludovic Maingault and Angélique Dauvin for animals'  
472 care and Florianne Michel for genotyping. We acknowledge the technical platform Functional  
473 and Physiological Exploration platform (FPE) of the Université Paris Cité, CNRS, Unité de  
474

Montalban et al.

475 Biologie Fonctionnelle et Adaptative, F-75013 Paris, France, the viral production facility of  
476 the UMR INSERM 1089 and the animal core facility “Buffon” of the Université Paris  
477 Cité/Institut Jacques Monod. We thank the animal facility of IBPS of Sorbonne Université,  
478 Paris.

479

480 **DECLARATION OF INTEREST**

481 "The authors declare no competing interests"

482

483 **FIGURES LEGENDS**

484 **Figure-1 DIO increases glial-fibrillary acidic protein (GFAP) immunoreactivity in**  
485 **the DS and the NAc. A Left-**Schematic representation of the protocol. **Right-**After  
486 190 days of HFHS diet obese mice showed a significant increase in fat mass as  
487 compared to lean. Unpaired Mann-Whitney test \*\*\*\* $p < 0.0001$ ,  $n = 24$  **B** Confocal  
488 images representative of GFAP immunoreactivity in the DS and the NAc of lean and  
489 DIO mice. **C-H** In the NAc and the DS, DIO increases relative expression of GFAP  
490 immunoreactivity compared to lean (**C, NAc; F, DS**). DIO also results in a decrease  
491 of astrocytes sphericity (**D-NAc**, unpaired t-test  $p = 0.0064$ /**G-DS** unpaired t-test  
492  $p < 0.0001$ ). Total surface of astrocytic coverage was decreased by DIO in NAc, **E-**  
493 **NAc**, unpaired t-test  $p < 0.0001$ , while was left unchanged in the DS **H-DS** unpaired t-  
494 test  $p = 0.2496$ ). All data are expressed as mean  $\pm$  SEM.  $n = 24$ , 6 mice in each group.  
495 **I-L** DIO increases  $Ca^{2+}$  strength and decreases the overall temporal correlation of  
496 astrocyte  $Ca^{2+}$  signal intensity in Glast-GCaMP6 mice expressing GCaMP  
497 selectively under the GLAST promoter (For NAc, Lean:  $n = 643$  active regions, 24  
498 slices, 6 mice; Obese:  $n = 586$  active regions, 19 slices, 4 mice; for DS, in Lean,  $n =$   
499  $204$  active regions, 11 slices, 4 mice; Obese,  $n = 178$  active regions, 8 slices, 3  
500 mice).

501

502

503 **Figure-2 DIO alter region specific astrocytic  $Ca^{2+}$  activity in the DS.** DIO  
504 decreases the overall temporal correlation of astrocyte  $Ca^{2+}$  signal intensity in Glast-  
505 GCaMP6 mice expressing GCaMP selectively under the GLAST promoter in the DS.  
506 Lean,  $n = 204$  active regions, 11 slices, 4 mice; Obese,  $n = 178$  active regions, 8  
507 slices, 3 mice. **A.** Representative pseudo-images of the GCaMP6 fluorescence  
508 projection of the spontaneous  $Ca^{2+}$  activity in the NAc of lean (top) and obese  
509 (middle) mice. Histogram data (bottom) are expressed as mean  $\pm$  SEM. Scale bar:  
510  $20 \mu m$  **B.** Distribution of temporal correlations of  $Ca^{2+}$  responses of all paired active  
511 domains (as an estimation of global synchronization) in lean (top) and obese  
512 (middle). Overall  $Ca^{2+}$  strength data (bottom) are expressed as mean  $\pm$  SEM.

513

514

515 **Figure-3 Activation of astrocytes augments neuronal activity synchrony in the**  
516 **DS in obese mice.**

517 **A.** Neuronal spontaneous activity was recorded by  $Ca^{2+}$  imaging with GCaMP6. *Left*,  
518 temporal projection of GCaMP6 fluorescence, scale bar,  $20 \mu m$ ; *middle*, identified regions  
519 displaying  $Ca^{2+}$  oscillations; *right*, raster plot showing GCaMP6 fluorescence fluctuations  
520 over time indicating the spontaneous  $Ca^{2+}$  signals. Scale bar,  $50 \mu m$ . Temporal bar, 10 s. **B.**  
521 Distribution of temporal correlation of neuronal  $Ca^{2+}$  signal between lean and obese mice.  
522 Temporal correlation was derived from the Pearson's correlation coefficients calculated  
523 between all pairs of individual  $Ca^{2+}$  signals. 6131 signal pairs for four mice for lean, and  
524 11796 pairs from three mice for obese condition. Wilcoxon rank sum (Mann-Whitney) test,  $p$   
525  $= 1.65 \times 10^{-6}$ ,  $h = 1$ , stats = [zval: 18.58, ranksum:  $6.1067 \times 10^7$ ]. **C.** Distribution of the  
526 temporal correlation of neuronal  $Ca^{2+}$  signals in response to astrocyte Gq DREADD  
527 activation in lean mice (9199 signal pairs from three mice). Lean and obese as referenced  
528 from **B**. **D.** In obese mice, astrocyte Gq DREADD activation by CNO enhanced the temporal  
529 correlation (synchrony) of neuronal  $Ca^{2+}$  signals (20326 signal pairs from three mice;  $p =$   
530  $6.97 \times 10^{-125}$ ,  $h = 1$ , stats = [zval: -23.7691, ranksum:  $1.7042 \times 10^8$ ]). **E.** Activation of



531 astrocyte Gq DREADD enhances neuronal  $\text{Ca}^{2+}$  intensity in lean ( $p = 1.06 \times 10^{-24}$ ,  $h = 1$ ,  
532 stats = [zval: -10.2608, ranksum: 4438]) and in obese (ranksum,  $p = 0.032$ ,  $h = 1$ , stats =  
533 [zval: -2.1403, ranksum: 82174]) mice. The  $\text{Ca}^{2+}$  strength derived from normalized temporal  
534 integral was compared for control (pre CNO) and CNO application phase (Lean, 89  
535 responsive regions, 3 slices, 3 mice; Obese: 294 regions, 5 slices, 3 mice).

536

537 **Figure-4 Effect of DS astrocytes activation on the reversal learning in a T-maze**  
538 **paradigm in Aldh111-cre lean and obese mice.** A) Right behavioral paradigm. Left

539 Performances of Aldh111<sup>DS-mCherry</sup> lean and obese mice were compared for learning  
540 and reversal learning skills. A significant between group difference in the reversal  
541 phase indicate a decreased flexibility in obese as compare to lean mice. Reversal

542 phase, two-way ANOVA Column Factor  $F(1, 14) = 33.80$   $P < 0.0001$  Data are  
543 expressed as mean  $\pm$  SEM.  $n = 8$ . **B.** DS<sup>mCherry</sup> and DS<sup>hM3Dq</sup> lean mice were trained in

544 a T-maze and injected with CNO before the reversal phase. CNO injections slightly  
545 increases flexibility in DS<sup>hM3Dq</sup> mice as compared to control. Group Factor  $F(1, 27) =$   
546  $5.125$   $P = 0.0318$ , Data are expressed as mean  $\pm$  SEM.  $n = 14-15$ . **C** Astrocytes

547 activation before the reversal phase in obese DS<sup>hM3Dq</sup> mice restore the behavioral  
548 performances. Two-way ANOVA: Group Factor  $(1, 12) = 35.54$   $P < 0.0001$  Data are  
549 expressed as mean  $\pm$  SEM.  $n = 7$ . **D-G** Neuronal  $\text{Ca}^{2+}$  activity was evaluated during

550 reversal learning by fiber photometry in the DS of DS<sup>mCherry</sup> and DS<sup>hM3Dq</sup> mice co-  
551 injected with a virus expressing GCaMP6f in DS neurons. Each mouse was injected  
552 with CNO 30 minutes before the test and recorded during the T-maze session. **D,F**

553 Peri-event heat map of the single trials of DS<sup>mCherry</sup> and DS<sup>hM3Dq</sup> mice respectively,  
554 aligned to the time when mice attained the baited arm. **E,G** Plot of area under the  
555 curve (AUC) during the baited arm exploration vs before turning in the baited arm (4 s

556 each, indicated by horizontal grey bars) in mice treated with CNO ( $n = 16$  and 39  
557 trials for DS<sup>mCherry</sup> and DS<sup>hM3Dq</sup> mice respectively). Statistical analysis two-tailed  
558 Mann-Whitney test,  $p = 0.74$  for DS<sup>mCherry</sup> and  $p = 0.0126$  for DS<sup>hM3Dq</sup> mice. **H-J** DA

559 transmission was evaluated by fiber photometry during reversal learning in DS of  
560 DS<sup>mCherry</sup> and DS<sup>hM3Dq</sup> mice co-injected with a virus expressing dLight-1 in DS  
561 neurons. Each mouse was recorded twice with an interval  $\geq 1$  day (Reversal day 1

562 and Reversal day 2), 30 min after receiving either vehicle (**Veh**) or misoprostol (**CNO**,  
563  $0.06 \text{ mg.kg}^{-1}$ , i.p.). **H,I** Peri-event heat map of single trials of mice injected with Veh or

564 CNO aligned to the time when mice attained the baited arm. Plot of area under the  
565 curve (AUC) during the baited arm exploration minus the AUC before turning in the  
566 baited arm (4 s, horizontal bars) in mice treated with Veh (RV1) vs CNO (RV2),  
567 Statistical analysis two-tailed Mann-Whitney test,  $p = 0.0360$  ( $n = 16$  and 29 trials for  
568 Veh and CNO respectively).

569

570 **Figure-5 DIO increases  $\text{Ca}^{2+}$  strength and decreases the overall temporal**  
571 **correlation of astrocyte  $\text{Ca}^{2+}$  signal intensity** in Glaxt-GCaMP6 mice expressing

572 GCaMP selectively under the GLAST promoter in the NAc. Lean:  $n = 643$  active  
573 regions, 24 slices, 6 mice; Obese:  $n = 586$  active regions, 19 slices, 4 mice. **A**

574 Coronal brain slice showing the colocalization of GFP signal (green) and S100b (red)  
575 immunostaining in GCaMP-GLAST mice. **B.** Representative pseudo-images of the  
576 GCaMP6 fluorescence projection of the spontaneous  $\text{Ca}^{2+}$  activity in the NAc of lean  
577 (top) and obese (middle) mice. Histogram data (bottom) are expressed as mean  $\pm$

578 SEM. **C.** Distribution of temporal correlations of  $\text{Ca}^{2+}$  responses of all paired active  
579 domains (as an estimation of global synchronization) in lean (top) and obese  
580 (middle). Overall  $\text{Ca}^{2+}$  strength data (bottom) are expressed as mean  $\pm$  SEM.

580

581

582

583

584

585

586

587

588

589

590

591

592

593

594

**Figure-6: Metabolic consequences of chemogenetic activation of Gq signaling in astrocytes of the NAc in lean and obese mice.** **A.** Schematic representation of the DIO paradigm. Astrocytes activation in  $\text{NAc}^{\text{hM3Dq}}$  mice fed with chow diet does not alter food intake **B** but decreases respiratory exchange ratio (RER) in  $\text{NAc}^{\text{hM3Dq}}$  mice fed with chow diet **C.** RER correlate with caloric intake for both  $\text{NAc}^{\text{mCherry}}$  and  $\text{NAc}^{\text{hM3Dq}}$  mice **D.** Astrocytes activation in lean  $\text{NAc}^{\text{hM3Dq}}$  mice increases fatty acid oxidation **E** and decreases energy expenditure (EE) **F.** EE does not correlate with LBM in neither  $\text{NAc}^{\text{mCherry}}$  mice or  $\text{NAc}^{\text{hM3Dq}}$  mice. **G.** Locomotion is not impacted by astrocytes activation **H.** Metabolic parameters are not impacted by CNO injection in obese  $\text{NAc}^{\text{mCherry}}$  and  $\text{NAc}^{\text{hM3Dq}}$  mice fed with HFHS diet. Cumulative caloric intake, FatOx, energy expenditure (EE) and respiratory exchange ratio (RER) are not significantly modified by CNO injection **I-L.** (N = 6 mice each group; VEH: vehicle).

595

596

## REFERENCES

597

598

599

600

Adams WK, Sussman JL, Kaur S, D'souza AM, Kieffer TJ, Winstanley CA (2015) Long-term, calorie-restricted intake of a high-fat diet in rats reduces impulse control and ventral striatal D2 receptor signalling - two markers of addiction vulnerability. *Eur J Neurosci* 42:3095–3104.

601

602

603

Agulhon C, Petravicz J, McMullen AB, Sweger EJ, Minton SK, Taves SR, Casper KB, Fiacco TA, McCarthy KD (2008) What is the role of astrocyte calcium in neurophysiology? *Neuron* 59:932–946.

604

605

Alcaro A, Huber R, Panksepp J (2007) Behavioral functions of the mesolimbic dopaminergic system: an affective neuroethological perspective. *Brain Res Rev* 56:283–321.

606

607

Araque A, Parpura V, Sanzgiri RP, Haydon PG (1999) Tripartite synapses: glia, the unacknowledged partner. *Trends Neurosci* 22:208–215.

608

609

610

Babbs RK, Sun X, Felsted J, Chouinard-Decorte F, Veldhuizen MG, Small DM (2013) Decreased caudate response to milkshake is associated with higher body mass index and greater impulsivity. *Physiol Behav* 121:103–111.

611

612

613

Baudonnat M, Huber A, David V, Walton M (2013) Heads for learning, tails for memory: reward, reinforcement and a role of dopamine in determining behavioral relevance across multiple timescales. *Frontiers in Neuroscience* 7.

614

615

Berland C et al. (2020) Circulating Triglycerides Gate Dopamine-Associated Behaviors through DRD2-Expressing Neurons. *Cell Metabolism* 31:773-790.e11.

616

617

Berridge KC (1996) Food reward: Brain substrates of wanting and liking. *Neuroscience & Biobehavioral Reviews* 20:1–25.

618

619

Berthoud H-R, Münzberg H, Morrison CD (2017) Blaming the Brain for Obesity: Integration of Hedonic and Homeostatic Mechanisms. *Gastroenterology* 152:1728–1738.

- 620 Björklund A, Dunnett SB (2007) Dopamine neuron systems in the brain: an update. Trends in  
621 Neurosciences 30:194–202.
- 622 Cahoy JD, Emery B, Kaushal A, Foo LC, Zamanian JL, Christopherson KS, Xing Y, Lubischer JL,  
623 Krieg PA, Krupenko SA, Thompson WJ, Barres BA (2008) A transcriptome database for  
624 astrocytes, neurons, and oligodendrocytes: a new resource for understanding brain  
625 development and function. J Neurosci 28:264–278.
- 626 Clyburn C, Browning KN (2019) Role of astroglia in diet-induced central neuroplasticity.  
627 Journal of Neurophysiology 121:1195–1206.
- 628 Corkrum M, Covelo A, Lines J, Bellocchio L, Pisansky M, Loke K, Quintana R, Rothwell PE,  
629 Lujan R, Marsicano G, Martin ED, Thomas MJ, Kofuji P, Araque A (2020) Dopamine-  
630 Evoked Synaptic Regulation in the Nucleus Accumbens Requires Astrocyte Activity.  
631 Neuron 0.
- 632 D’Ascenzo M, Fellin T, Terunuma M, Revilla-Sanchez R, Meaney DF, Auberson YP, Moss SJ,  
633 Haydon PG (2007) mGluR5 stimulates gliotransmission in the nucleus accumbens.  
634 Proc Natl Acad Sci U S A 104:1995–2000.
- 635 Douglass JD, Dorfman MD, Fasnacht R, Shaffer LD, Thaler JP (2017) Astrocyte IKKbeta/NF-  
636 kappaB signaling is required for diet-induced obesity and hypothalamic inflammation.  
637 Mol Metab 6:366–373.
- 638 Escartin C et al. (2021) Reactive astrocyte nomenclature, definitions, and future directions.  
639 Nat Neurosci 24:312–325.
- 640 Farzi A, Lau J, Ip CK, Qi Y, Shi Y-C, Zhang L, Tasan R, Sperk G, Herzog H (2018) Arcuate nucleus  
641 and lateral hypothalamic CART neurons in the mouse brain exert opposing effects on  
642 energy expenditure Elmquist JK, Dulac C, eds. eLife 7:e36494.
- 643 Fellin T, Pascual O, Gobbo S, Pozzan T, Haydon PG, Carmignoto G (2004) Neuronal synchrony  
644 mediated by astrocytic glutamate through activation of extrasynaptic NMDA  
645 receptors. Neuron 43:729–743.
- 646 Foldi CJ, Morris MJ, Oldfield BJ (2021) Executive function in obesity and anorexia nervosa:  
647 Opposite ends of a spectrum of disordered feeding behaviour? Progress in Neuro-  
648 Psychopharmacology and Biological Psychiatry 111:110395.
- 649 García-Cáceres C, Balland E, Prevot V, Luquet S, Woods SC, Koch M, Horvath TL, Yi C-X,  
650 Chowen JA, Verkhatsky A, Araque A, Bechmann I, Tschöp MH (2019) Role of  
651 astrocytes, microglia, and tanocytes in brain control of systemic metabolism. Nature  
652 Neuroscience 22:7–14.
- 653 GBD 2015 Obesity Collaborators et al. (2017) Health Effects of Overweight and Obesity in  
654 195 Countries over 25 Years. N Engl J Med 377:13–27.
- 655 Herrera Moro Chao D, Kirchner MK, Pham C, Foppen E, Denis RGP, Castel J, Morel C,  
656 Montalban E, Hassouna R, Bui L-C, Renault J, Mouffle C, García-Cáceres C, Tschöp

- 657 MH, Li D, Martin C, Stern JE, Luquet SH (2022) Hypothalamic astrocytes control  
658 systemic glucose metabolism and energy balance. *Cell Metabolism* 34:1532-1547.e6.
- 659 Howe MW, Atallah HE, McCool A, Gibson DJ, Graybiel AM (2011) Habit learning is associated  
660 with major shifts in frequencies of oscillatory activity and synchronized spike firing in  
661 striatum. *Proc Natl Acad Sci U S A* 108:16801–16806.
- 662 Insel T, Cuthbert B, Garvey M, Heinssen R, Pine DS, Quinn K, Sanislow C, Wang P (2010)  
663 Research domain criteria (RDoC): toward a new classification framework for research  
664 on mental disorders. *Am J Psychiatry* 167:748–751.
- 665 Isaacson J (1999) Glutamate spillover mediates excitatory transmission in the rat olfactory  
666 bulb. *Neuron* 23:377–384.
- 667 Izquierdo A, Brigman JL, Radke AK, Rudebeck PH, Holmes A (2017) The neural basis of  
668 reversal learning: An updated perspective. *Neuroscience* 345:12–26.
- 669 Jocham G, Klein TA, Neumann J, Cramon DY von, Reuter M, Ullsperger M (2009) Dopamine  
670 DRD2 Polymorphism Alters Reversal Learning and Associated Neural Activity. *J*  
671 *Neurosci* 29:3695–3704.
- 672 Johnson PM, Kenny PJ (2010) Dopamine D2 receptors in addiction-like reward dysfunction  
673 and compulsive eating in obese rats. *Nat Neurosci* 13:635–641.
- 674 Kang S, Hong S-I, Lee J, Peyton L, Baker M, Choi S, Kim H, Chang S-Y, Choi D-S (2020)  
675 Activation of Astrocytes in the Dorsomedial Striatum Facilitates Transition From  
676 Habitual to Goal-Directed Reward-Seeking Behavior. *Biological Psychiatry* 88:797–  
677 808.
- 678 Kelley AE, Baldo BA, Pratt WE (2005) A proposed hypothalamic-thalamic-striatal axis for the  
679 integration of energy balance, arousal, and food reward. *J Comp Neurol* 493:72–85.
- 680 Kempadoo KA, Tourino C, Cho SL, Magnani F, Leininger G-M, Stuber GD, Zhang F, Myers  
681 MG, Deisseroth K, de Lecea L, Bonci A (2013) Hypothalamic neurotensin projections  
682 promote reward by enhancing glutamate transmission in the VTA. *J Neurosci*  
683 33:7618–7626.
- 684 Kenny PJ (2011) Common cellular and molecular mechanisms in obesity and drug addiction.  
685 *Nat Rev Neurosci* 12:638–651.
- 686 Khakh BS, McCarthy KD (2015) Astrocyte Calcium Signaling: From Observations to Functions  
687 and the Challenges Therein. *Cold Spring Harb Perspect Biol*.
- 688 Khakh BS, Sofroniew MV (2015) Diversity of astrocyte functions and phenotypes in neural  
689 circuits. *Nat Neurosci* 18:942–952.
- 690 Koob GF, Volkow ND (2010) Neurocircuitry of Addiction. *Neuropsychopharmacol* 35:217–  
691 238.

- 692 Kravitz AV, Kreitzer AC (2012) Striatal Mechanisms Underlying Movement, Reinforcement,  
693 and Punishment. *Physiology (Bethesda)* 27:10.1152/physiol.00004.2012.
- 694 Lee D, Seo H, Jung MW (2012) Neural Basis of Reinforcement Learning and Decision Making.  
695 *Annual Review of Neuroscience* 35:287–308.
- 696 Lenoir M, Serre F, Cantin L, Ahmed SH (2007) Intense Sweetness Surpasses Cocaine Reward.  
697 *PLOS ONE* 2:e698.
- 698 Leroi I, Barraclough M, McKie S, Hinest N, Evans J, Elliott R, McDonald K (2013)  
699 Dopaminergic influences on executive function and impulsive behaviour in impulse  
700 control disorders in Parkinson’s disease. *J Neuropsychol* 7:306–325.
- 701 Leybaert L, Sanderson MJ (2012) Intercellular Ca<sup>2+</sup> Waves: Mechanisms and Function.  
702 *Physiological Reviews* 92:1359–1392.
- 703 Martin C, Houitte D, Guillermier M, Petit F, Bonvento G, Gurden H (2012) Alteration of  
704 sensory-evoked metabolic and oscillatory activities in the olfactory bulb of GLAST-  
705 deficient mice. *Front Neural Circuits* 6:1.
- 706 Martín R, Bajo-Grañeras R, Moratalla R, Perea G, Araque A (2015) Circuit-specific signaling in  
707 astrocyte-neuron networks in basal ganglia pathways. *Science* 349:730–734.
- 708 Michaelides M, Thanos PK, Volkow ND, Wang G-J (2012) Dopamine-related frontostriatal  
709 abnormalities in obesity and binge-eating disorder: emerging evidence for  
710 developmental psychopathology. *Int Rev Psychiatry* 24:211–218.
- 711 Montalban E et al. (2022) Translational profiling of mouse dopaminoceptive neurons reveals  
712 region-specific gene expression, exon usage, and striatal prostaglandin E2  
713 modulatory effects. *Mol Psychiatry* 27:2068–2079.
- 714 Montalban E et al. (2023) The addiction-susceptibility Taq1A/Ankyrin repeat and kinase  
715 domain containing 1 kinase (ANKK1) controls reward and metabolism through  
716 dopamine receptor type 2 (D2R)-expressing neurons. *Biological Psychiatry* 0.
- 717 Must A, Spadano J, Coakley EH, Field AE, Colditz G, Dietz WH (1999) The disease burden  
718 associated with overweight and obesity. *JAMA* 282:1523–1529.
- 719 O’Connor EC, Kremer Y, Lefort S, Harada M, Pascoli V, Rohner C, Lüscher C (2015) Accumbal  
720 D1R Neurons Projecting to Lateral Hypothalamus Authorize Feeding. *Neuron* 88:553–  
721 564.
- 722 Oliveira JF, Araque A (2022) Astrocyte regulation of neural circuit activity and network  
723 states. *Glia* 70:1455–1466.
- 724 Oliveira MGM, Bueno OFA, Pomarico AC, Gugliano EB (1997) Strategies Used by  
725 Hippocampal- and Caudate-Putamen-Lesioned Rats in a Learning Task. *Neurobiology*  
726 *of Learning and Memory* 68:32–41.

- 727 Orellana JA, Retamal MA, Moraga-Amaro R, Stehberg J (2016) Role of Astroglial  
728 Hemichannels and Pannexons in Memory and Neurodegenerative Diseases. *Front*  
729 *Integr Neurosci* 10.
- 730 Patriarchi T, Cho JR, Merten K, Howe MW, Marley A, Xiong W-H, Folk RW, Broussard GJ,  
731 Liang R, Jang MJ, Zhong H, Dombeck D, von Zastrow M, Nimmerjahn A, Gradinaru V,  
732 Williams JT, Tian L (2018) Ultrafast neuronal imaging of dopamine dynamics with  
733 designed genetically encoded sensors. *Science* 360.
- 734 Pham C, Moro DH, Mouffle C, Didienne S, Hepp R, Pfrieder FW, Mangin J-M, Legendre P,  
735 Martin C, Luquet S, Cauli B, Li D (2020) Mapping astrocyte activity domains by light  
736 sheet imaging and spatio-temporal correlation screening. *Neuroimage* 220:117069.
- 737 Poskanzer KE, Yuste R (2011) Astrocytic regulation of cortical UP states. *Proceedings of the*  
738 *National Academy of Sciences* 108:18453–18458.
- 739 Poskanzer KE, Yuste R (2016) Astrocytes regulate cortical state switching in vivo. *PNAS*  
740 113:E2675–E2684.
- 741 Roberts BM, Lambert E, Livesey JA, Wu Z, Li Y, Cragg SJ (2022) Dopamine Release in Nucleus  
742 Accumbens Is under Tonic Inhibition by Adenosine A1 Receptors Regulated by  
743 Astrocytic ENT1 and Dysregulated by Ethanol. *J Neurosci* 42:1738–1751.
- 744 Savtchouk I, Volterra A (2018) Gliotransmission: Beyond Black-and-White. *J Neurosci* 38:14–  
745 25.
- 746 Seabrook LT, Naef L, Baimel C, Judge AK, Kenney T, Ellis M, Tayyab T, Armstrong M, Qiao M,  
747 Floresco SB, Borgland SL (2023) Disinhibition of the orbitofrontal cortex biases  
748 decision-making in obesity. *Nat Neurosci* 26:92–106.
- 749 Sears RM, Liu R-J, Narayanan NS, Sharf R, Yeckel MF, Laubach M, Aghajanian GK, DiLeone RJ  
750 (2010) Regulation of nucleus accumbens activity by the hypothalamic neuropeptide  
751 melanin-concentrating hormone. *J Neurosci* 30:8263–8273.
- 752 Smith KS, Graybiel AM (2016) Habit formation coincides with shifts in reinforcement  
753 representations in the sensorimotor striatum. *J Neurophysiol* 115:1487–1498.
- 754 Stice E, Spoor S, Bohon C, Small DM (2008) Relation Between Obesity and Blunted Striatal  
755 Response to Food Is Moderated by Taq1A A1 Allele. *Science* 322:449–452.
- 756 Stratford TR, Kelley AE (1999) Evidence of a Functional Relationship between the Nucleus  
757 Accumbens Shell and Lateral Hypothalamus Subserving the Control of Feeding  
758 Behavior. *J Neurosci* 19:11040–11048.
- 759 Tellez LA, Medina S, Han W, Ferreira JG, Licon-Limón P, Ren X, Lam TT, Schwartz GJ, De  
760 Araujo IE (2013) A gut lipid messenger links excess dietary fat to dopamine  
761 deficiency. *Science* 341:800–802.
- 762 Ter Horst KW, Lammers NM, Trinko R, Opland DM, Figeo M, Ackermans MT, Booij J, van den  
763 Munckhof P, Schuurman PR, Fliers E, Denys D, DiLeone RJ, la Fleur SE, Serlie MJ

- 764 (2018) Striatal dopamine regulates systemic glucose metabolism in humans and mice.  
765 Sci Transl Med 10:eaar3752.
- 766 Thaler JP, Yi C-X, Schur EA, Guyenet SJ, Hwang BH, Dietrich MO, Zhao X, Sarruf DA, Izgur V,  
767 Maravilla KR, Nguyen HT, Fischer JD, Matsen ME, Wisse BE, Morton GJ, Horvath TL,  
768 Baskin DG, Tschöp MH, Schwartz MW (2012) Obesity is associated with hypothalamic  
769 injury in rodents and humans. J Clin Invest 122:153–162.
- 770 Thoeni S, Loureiro M, O'Connor EC, Lüscher C (2020) Depression of Accumbal to Lateral  
771 Hypothalamic Synapses Gates Overeating. Neuron 107:158-172.e4.
- 772 Thorn CA, Graybiel AM (2014) Differential entrainment and learning-related dynamics of  
773 spike and local field potential activity in the sensorimotor and associative striatum. J  
774 Neurosci 34:2845–2859.
- 775 Uhlhaas PJ, Singer W (2006) Neural synchrony in brain disorders: relevance for cognitive  
776 dysfunctions and pathophysiology. Neuron 52:155–168.
- 777 Valtcheva S, Venance L (2016) Astrocytes gate Hebbian synaptic plasticity in the striatum.  
778 Nat Commun 7:13845.
- 779 van Elzelingen W, Warnaar P, Matos J, Bastet W, Jonkman R, Smulders D, Goedhoop J, Denys  
780 D, Arbab T, Willuhn I (2022) Striatal dopamine signals are region specific and  
781 temporally stable across action-sequence habit formation. Curr Biol 32:1163-  
782 1174.e6.
- 783 Volkow ND, Wise RA (2005) How can drug addiction help us understand obesity? Nat  
784 Neurosci 8:555–560.
- 785 Wang GJ, Volkow ND, Logan J, Pappas NR, Wong CT, Zhu W, Netusil N, Fowler JS (2001) Brain  
786 dopamine and obesity. Lancet 357:354–357.
- 787 Watson DJ, Stanton ME (2009) Spatial discrimination reversal learning in weanling rats is  
788 impaired by striatal administration of an NMDA-receptor antagonist. Learn Mem  
789 16:564–572.
- 790 Yang Y, Shields GS, Guo C, Liu Y (2018) Executive function performance in obesity and  
791 overweight individuals: A meta-analysis and review. Neurosci Biobehav Rev 84:225–  
792 244.
- 793  
794

795 **METHODS**

796

797 **Experimental models and subject details**

798 **Animal studies**

799 All animal protocols were approved by the Animal Care Committee of the University of Paris  
800 (APAFIS #2015062611174320), or the Institut Biologie Paris Seine of Sorbonne University  
801 (C75-05-24). Twelve to fifteen-week-old male Aldh1-L1-Cre (Tg(Aldh1l1-cre) JD1884Htz,  
802 Jackson laboratory, Bar Harbor, USA), male C57BL/6J (Janvier, Le Genest St-Isle, France)  
803 or male GCaMP6f/Glast-CreERT2 (Pham et al., 2020) mice were individually housed at  
804 constant temperature (23± 2°C) and submitted to a 12/12h light/dark cycle. All mice had  
805 access to regular chow diet (Safe, Augy, France) and water ad libitum, unless stated  
806 otherwise. Additionally, age matched C57BL/6J, GCaMP6f/Glast-CreERT2 or Aldh1-L1-Cre  
807 mice groups were fed with either chow diet or high-fat high-sugar diet (HFHS, cat n. D12451,  
808 Research Diets, New Brunswick, USA) for twelve to sixteen weeks. Body weight was  
809 measured every week and body weight gain was estimated as the difference of body weight  
810 in week one of HFHS diet consumption to twelve to sixteen weeks after HFHS diet exposure.

811

812 **Viral constructs**

813 Designer receptor exclusively activated by designer drugs (DREADD) and GCaMP6f viruses  
814 were purchased from <http://www.addgene.org/>, unless stated otherwise. pAAV-EF1α-DIO-  
815 hM3Dq-mCherry (2.4x10<sup>12</sup> vg/ml, Addgene plasmid #50460-AAV5;  
816 <http://www.addgene.org/50460/>; RRID: Addgene\_50460), pAAV-EF1α-DIO-mCherry  
817 (3.6x10<sup>12</sup> vg/ml, Addgene plasmid #50462-AAV5; <http://www.addgene.org/50462/>; RRID:  
818 Addgene\_50462), pAAV-EF1a-DIO-hM3D(Gq)-mCherry was a gift from Bryan Roth  
819 (Addgene plasmid # 50460; <http://n2t.net/addgene:50460>; RRID: Addgene\_50460). pAAV-  
820 CAG-Flex.GCaMP6f.WPRE (3.15x10<sup>13</sup> vg/ml, working dilution 1:10, Addgene plasmid  
821 #100835-AAV5; <http://www.addgene.org/100835/>; RRID:Addgene\_100835) was a gift of  
822 Douglas Kim and GENIE Project. pAAV-GfaACC1D.Lck-GCaMP6f.SV40 (1.53x10<sup>13</sup> vg/ml,  
823 working dilution 1:5, Addgene plasmid #52925-AAV5; <http://www.addgene.org/52295/>; RRID:  
824 Addgene\_52925) was a gift of Baljit Khak. pAAV-CAG-dLight1.1 was a gift from Lin Tian  
825 (Addgene viral prep # 111067-AAV5; <http://n2t.net/addgene:111067>; RRID:  
826 Addgene\_111067)

827

828 **Surgical procedures**

829 For all surgical procedures, mice were first intraperitoneal (ip) injected with the analgesic  
830 Buprenorphine (Buprecare, 0.3 mg/kg, Recipharm, Lancashire, UK). 30 minutes after the  
831 injection mice were rapidly anesthetized with isoflurane (3%), intraperitoneal (ip) injected with



832 the analgesic Buprenorphine (Buprecare, 0.3 mg/kg, Recipharm, Lancashire, UK) and  
833 Ketoprofen (Ketofen, 10 mg/kg, France) and maintained under 1.5% isoflurane anesthesia  
834 throughout the surgery.

835 Stereotaxic surgery. Male Aldh1-L1-Cre+/-, Aldh1-L1-Cre-/- and male C57BL/6J mice were  
836 placed on a stereotactic frame (David Kopf Instruments, California, USA) and bilateral viral  
837 injections were performed with 0.6ul in DS (stereotaxic coordinates: L = +/-1.75; AP = +0.6; V  
838 = -3.5, and -3 in mm), or 0.3ul in NAc (L=+/- 1; AP=+1.55, V=-4.5) at a rate of 50 nl.min<sup>-1</sup>.  
839 The injection needle was carefully removed after 5 min waiting at the injection site and 2 min  
840 waiting half way to the top. Mice recovered for at least 3 weeks after the surgery before being  
841 involved in experimental procedures.

842

### 843 **Behavioral assays**

844 **Haloperidol-induced catalepsy.** Mice were injected with haloperidol (0.5 mg.kg<sup>-1</sup>, i.p.).  
845 Catalepsy was measured at several time points, 45-180 min after haloperidol injection.  
846 Animals were taken out of their home cage and placed in front of a 4-cm elevated steel bar,  
847 with the forelegs upon the bar and hind legs remaining on the ground surface. The time  
848 during which animals remained still was measured. A behavioral threshold of 180 seconds  
849 was set so the animals remaining in the cataleptic position for this duration were put back in  
850 their cage until the next time point.

851 **T-maze.** Mice were tested for learning and cognitive flexibility in a gray T maze (arm 35-cm  
852 length, 25-cm height, 15-cm width). All mice were mildly food deprived (85-90 % of original  
853 weight) for 3 days prior to starting the experiment. The first day mice were placed in the  
854 maze for 15 min for habituation. Then, mice underwent 3 days of training with one arm  
855 reinforced with a highly palatable food pellet (HFHS, cat n. D12451 Research Diet). Each  
856 mouse was placed at a start point and allowed to explore the maze. It was then blocked for  
857 20 seconds in the explored arm and then placed again in the starting arm. This process was  
858 repeated 10 times per day. At the end of the learning phase all mice showed a > 70 %  
859 preference for the reinforced arm. The average number of entries in each arm over 5 trials  
860 was plotted. Two days of reversal learning followed the training phase during which the  
861 reinforced arm was changed and the mice were subjected to 10 trials per day with the reward  
862 in the arm opposite to the previously baited one.

863 **SKF-induced locomotor activity.** Mice were placed in an automated online measurement  
864 system using an infrared beam-based activity monitoring system (Phenomaster, TSE  
865 Systems GmbH, Bad Homburg, Germany). After 1 day of habituation, mice were first i.p.  
866 injected with CNO (0.6 mg/Kg) and 30 minutes after with SKF-81297 (3□mg/kg), and placed  
867 back in the chamber for at least 80 minutes. Locomotion was recorded using an infrared

868 beam-based activity monitoring system Phenomaster, TSE Systems GmbH, Bad Homburg,  
869 Germany).

870

### 871 **Fiber photometry**

872 Aldh1-L1-Cre mice were anaesthetized with isoflurane and received 10 mg.kg<sup>-1</sup>  
873 intraperitoneal injection (i.p.) of Buprécare® (buprenorphine 0.3 mg) diluted 1/100 in NaCl 9  
874 g.L<sup>-1</sup> and 10 mg.kg<sup>-1</sup> of Ketofen® (ketoprofen 100 mg) diluted 1/100 in NaCl 9 g.L<sup>-1</sup>, and  
875 placed on a stereotactic frame (Model 940, David Kopf Instruments, California). We  
876 unilaterally injected 0.6 µl of virus (pAAV.Syn.Flex.GCaMP6f.WPRE.SV40, Addgene viral  
877 prep #100833-AAV9, titer ≥ 10<sup>13</sup> genome copy (GC).mL<sup>-1</sup>, working dilution 1:5) or d-Light1  
878 (pAAV-CAG-dLight1.1, Addgene viral prep # 111067-AAV5, titer ≥ 7×10<sup>12</sup> vg/mL, working  
879 dilution 1:1) into the DS (L = +/-1.5; AP = +0.86; V = -3.25, in mm) at a rate of 50 nl.min<sup>-1</sup>.  
880 The injection needle was carefully removed after 5 min waiting at the injection site and 2 min  
881 waiting half way to the top. Optical fiber for calcium imaging into the striatum was implanted  
882 100 µm above the viral injection site. A chronically implantable cannula (Doric Lenses,  
883 Québec, Canada) composed of a bare optical fiber (400 µm core, 0.48 N.A.) and a fiber  
884 ferrule was implanted 100 µm above the location of the viral injection site in the DS (L = +/-  
885 1.75; AP = +0.6; V = -3.5, and -3 in mm). The fiber was fixed onto the skull using dental  
886 cement (Super-Bond C&B, Sun Medical). Real time fluorescence emitted from the calcium  
887 sensor GCaMP6f expressed by astrocytes with the Aldh1-L1-Cre receptor was recorded  
888 using fiber photometry as described in (Berland et al., 2020). Fluorescence was collected in  
889 the DS using a single optical fiber for both delivery of excitation light streams and collection  
890 of emitted fluorescence. The fiber photometry setup used 2 light emitting LEDs: 405 nm LED  
891 sinusoidally modulated at 330 Hz and a 465 nm LED sinusoidally modulated at 533 Hz (Doric  
892 Lenses) merged in a FMC4 MiniCube (Doric Lenses) that combines the 2 wavelengths  
893 excitation light streams and separate them from the emission light. The MiniCube was  
894 connected to a fiber optic rotary joint (Doric Lenses) connected to the cannula. A RZ5P lock-  
895 in digital processor controlled by the Synapse software (Tucker-Davis Technologies, TDT,  
896 USA), commanded the voltage signal sent to the emitting LEDs via the LED driver (Doric  
897 Lenses). The light power before entering the implanted cannula was measured with a power  
898 meter (PM100USB, Thorlabs) before the beginning of each recording session. The light  
899 intensity to capture fluorescence emitted by 465 nm excitation was between 25-40 µW, for  
900 the 405 nm excitation this was between 10-20 µW at the tip of the fiber. The fluorescence  
901 emitted by the GCaMP6f activation in response to light excitation was collected by a  
902 femtowatt photoreceiver module (Doric Lenses) through the same fiber patch cord. The  
903 signal was then received by the RZ5P processor (TDT). On-line real time demodulation of  
904 the fluorescence due to the 405 nm and 465 nm excitations was performed by the Synapse

905 software (TDT). A camera was synchronized with the recording using the Synapse software.  
906 Signals were exported to MATLAB R2016b (Mathworks) and analyzed offline. After careful  
907 visual examination of all trials, they were clean of artifacts in these time intervals. The timing  
908 of events was extracted from the video. For each session, signal analysis was performed on  
909 two-time intervals: one extending from -4 to 0 sec (before entering the reinforced arm) and  
910 the other from 0 to +4 sec (reinforced arm). From a reference window (from -180 to -60 sec),  
911 a least-squares linear fit was applied to the 405 nm signal to align it to the 465 nm signal,  
912 producing a fitted 405 nm signal. This was then used to calculate the  $\Delta F/F$  that was used to  
913 normalize the 465 nm signal during the test window as follows:  $\Delta F/F = (465 \text{ nm signal}_{\text{test}} -$   
914  $\text{fitted } 405 \text{ nm signal}_{\text{ref}})/\text{fitted } 405 \text{ nm signal}_{\text{ref}}$ . To compare signal variations between the two  
915 conditions (before vs after entering the reinforced arm), for each mouse, the value  
916 corresponding to the entry point of the animal in the reinforced arm was set at zero.

917

#### 918 **Indirect calorimetry analysis**

919 All mice were monitored for metabolic efficiency (Labmaster, TSE Systems GmbH, Bad  
920 Homburg, Germany). After an initial period of acclimation in the calorimetry cages of at least  
921 two days, food and water intake, whole energy expenditure (EE), oxygen consumption and  
922 carbon dioxide production, respiratory quotient ( $RQ = V_{CO2}/V_{O2}$ , where V is volume) and  
923 locomotor activity were recorded as previously described<sup>83</sup>. Additionally, fatty acid oxidation  
924 was calculated as previously reported<sup>83</sup>. Reported data are the results of the average of the  
925 last three days of recording. Before and after indirect calorimetry assessment, body mass  
926 composition was analyzed using an Echo Medical systems' EchoMRI (Whole Body  
927 Composition Analyzers, EchoMRI, Houston, USA).

928

#### 929 **Ex-vivo calcium imaging**

930 Male Aldh1-L1-Cre<sup>+/-</sup> or C57BL/6J mice previously injected with GCaMP6f and DREADDs  
931 viral constructs, and GCaMP6f/Glast-CreERT2 mice were terminally anaesthetized using  
932 isoflurane. Brains were removed and placed in ice-cold oxygenated slicing artificial  
933 cerebrospinal solution (aCSF, 30mM NaCl, 4.5mM KCl, 1.2mM NaH<sub>2</sub>PO<sub>4</sub>, 1mM MgCl<sub>2</sub>,  
934 26mM NaHCO<sub>3</sub>, and 10mM D-Glucose and 194mM Sucrose) and subsequently cut into 300-  
935  $\mu\text{m}$  thick PVN coronal slices using a vibratome (Leica VT1200S, Nussloch, Germany). Next,  
936 brain slices were recovered in aCSF (124mM NaCl, 4.5mM KCl, 1.2mM NaH<sub>2</sub>PO<sub>4</sub>, 1mM  
937 MgCl<sub>2</sub>, 2mM CaCl<sub>2</sub>, 26mM NaHCO<sub>3</sub>, and 10mM D-Glucose) at 37 °C for 60 minutes.  
938 Imaging was carried out at room temperature under constant perfusion (~3 ml/min) of  
939 oxygenated aCSF. The overall cellular fluorescence of astrocytes expressing GCaMP6f was

940 collected by epifluorescence illumination. A narrow-band monochromator light source  
941 (Polychrome II, TILL Photonics, Germany) was directly coupled to the imaging objective via  
942 an optical fiber. Fluorescence signal was collected with a 40x 0.8NA or a 63x 1.0NA water  
943 immersion objective (Zeiss, Germany) and a digital electron-multiplying charge-coupled  
944 device (EMCCD Cascade 512B, Photometrics, Birmingham, UK) as previously described  
945 (Pham et al., 2020)(Pham, 2020). A double-band dichroic/filter set was used to reflect the  
946 excitation wavelength (470 nm) to slices and filter the emitted GCaMP6 green fluorescence  
947 (Di03-R488/561-t3; FF01-523/610, Semrock). The same filter was used for slices expressing  
948 both GCaMP6f and DREADD-mCherry. Striatal slices were transferred to the imaging  
949 chamber, where 3-minute astrocyte spontaneous activity recordings were performed in slices  
950 of GCaMP6f/Glast-CreERT2 mice. In the case of striatal slices of Aldh1-L1-Cre+/- and  
951 C57BL/6J mice, we performed a basal epifluorescence recording (60 seconds), followed by a  
952 120 second bath application of CNO (10 $\mu$ M) or Glutamate (30 $\mu$ M) and 240 seconds recording  
953 over the washing of the compounds.

954 The responsive regions displaying Ca<sup>2+</sup> signals were scrutinized by the three-dimensional  
955 spatio-temporal correlation screening method (Pham et al., 2020). Background signal was  
956 subtracted from the raw images by using the minimal intensity projection of the entire stack.  
957 Ca<sup>2+</sup> signals of individual responsive regions were normalized as dF/F<sub>0</sub>, with F<sub>0</sub> representing  
958 the baseline intensity and quantified using Matlab (The MathWorks, France) and Igor Pro  
959 (Wavemetrics, USA). We gauged signal strength of Ca<sup>2+</sup> traces of single responsive regions  
960 by calculating their temporal integration and normalizing per minute. The global temporal  
961 synchronization of detected Ca<sup>2+</sup> signals was determined by the temporal Pearson's  
962 correlation coefficients of all combinations between single Ca<sup>2+</sup> regions (Pham et al., 2020).

963

#### 964 **Brain tissue Immunofluorescence**

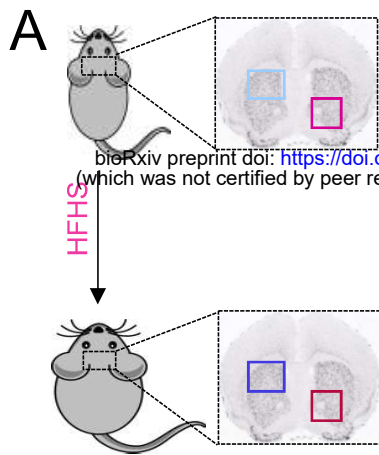
965 Mice were euthanized with pentobarbital (500 mg/kg, Dolethal, Vetoquinol, France) and  
966 transcardially perfused with 0.1 M sodium phosphate buffer (PBS, pH 7.5) followed by 4%  
967 paraformaldehyde in phosphate buffer (0.1 M, pH 7.2). Brains were removed and post-fixed  
968 overnight in 4% paraformaldehyde. Afterwards, the brains were transferred to 30% sucrose  
969 in PBS for 2 days for cryoprotection. Next, 30  $\mu$ m brain sections were cut in a freezing  
970 cryostat (Leica, Wetzlar, Germany) and further processed for immunofluorescence following  
971 the procedure previously described (Berland et al., 2020). Free-floating brain sections were  
972 incubated at 4°C overnight with mouse anti-Glial fibrillary acidic protein (GFAP, 1:1000,  
973 Sigma-Aldrich, Saint-Louis, USA) or mCherry (ab125096; 1:1000, Abcam, Cambridge, MA)  
974 primary antibodies. The next day, sections were rinsed in Tris-buffered saline (TBS, 0.25M  
975 Tris and 0.5M NaCl, pH 7.5) and incubated for 2 hours with secondary antibodies (1:1000,  
976 Thermo fisher Scientific, MA, USA) conjugated with fluorescent dyes: goat anti-chicken Alexa

977 488, donkey anti-rabbit Alexa 594, donkey anti-mouse Alexa 488 and donkey anti-rabbit  
978 Alexa 647. After rinsing, the sections were mounted and coverslipped with DAPI  
979 (Vectashield, Burlingade, California, USA) and examined with a confocal laser scanning  
980 microscope (Zeiss LSM 510, Oberkochen, Germany) with a color digital camera and  
981 AxioVision 3.0 imaging software.

982

### 983 **Statistical analyses**

984 Compiled data are always reported and represented as mean  $\pm$  s.e.m., with single data  
985 points plotted. Data were statistically analyzed with GraphPad Prism 9. Normal distribution  
986 was tested with Shapiro-Wilk test. When n was  $> 7$  and normality test passed, data were  
987 analyzed with Student's t test, one-way ANOVA, two-way ANOVA or repeated-measures  
988 ANOVA, as applicable and Holm-Sidak's post-hoc tests for two by two comparisons.  
989 Otherwise non-parametric Mann-Whitney test. All tests were two-tailed. Significance was  
990 considered as  $p < 0.05$ .



bioRxiv preprint doi: <https://doi.org/10.1101/2023.03.21.533596>; this version posted March 21, 2023. The copyright holder for this preprint (which was not certified by peer review) is the author/funder, who has granted bioRxiv a license to display the preprint in perpetuity. It is made available under aCC-BY-NC-ND 4.0 International license.

